Cell Reports

Article

Awake hippocampal synchronous events are incorporated into offline neuronal reactivation

Graphical abstract

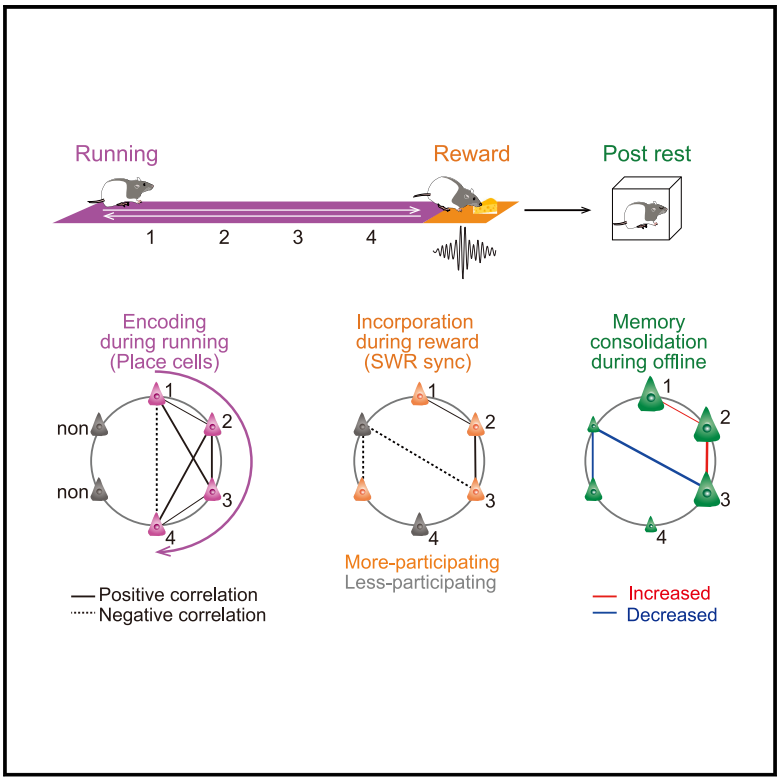

Authors

Saichiro Yagi, Hideyoshi Igata, Yuji Ikegaya, Takuya Sasaki

Correspondence

takuya.sasaki.b4@tohoku.ac.jp

In brief

Yagi et al. find that awake synchronous spike patterns are preferentially incorporated into post-experience neuronal reactivation in the hippocampus. This study proposes a role for awake synchronous events in the extraction of neuronal spike patterns for subsequent neuronal reactivation.

Highlights

- Awake hippocampal ripples are necessary for post-experience neuronal reactivation
- Awake synchronous spike patterns are represented in post-experience reactivation
- Place cells recruited in synchronization contribute to post-experience reactivation

Yagi et al., 2023, Cell Reports *42*, 112871
August 29, 2023
https://doi.org/10.1016/j.celrep.2023.112871

CellPress

Cell Reports

CellPress
OPEN ACCESS

Article

Awake hippocampal synchronous events are incorporated into offline neuronal reactivation

Saichiro Yagi,[1] Hideyoshi Igata,[1] Yuji Ikegaya,[1,2,3] and Takuya Sasaki[1,4,5,*]

[1]Laboratory of Chemical Pharmacology, Graduate School of Pharmaceutical Sciences, The University of Tokyo, Tokyo 113-0033, Japan
[2]Institute for AI and Beyond, The University of Tokyo, Tokyo 113-0033, Japan
[3]Center for Information and Neural Networks, National Institute of Information and Communications Technology, Suita City, Osaka 565-0871, Japan
[4]Department of Pharmacology, Graduate School of Pharmaceutical Sciences, Tohoku University, 6-3 Aramaki-Aoba, Aoba-Ku, Sendai 980-8578, Japan
[5]Lead contact
*Correspondence: takuya.sasaki.b4@tohoku.ac.jp
https://doi.org/10.1016/j.celrep.2023.112871

SUMMARY

Learning novel experiences reorganizes hippocampal neuronal circuits, represented as coordinated reactivation patterns in post-experience offline states for memory consolidation. This study examines how awake synchronous events during a novel run are related to post-run reactivation patterns. The disruption of awake sharp-wave ripples inhibited experience-induced increases in the contributions of neurons to post-experience synchronous events. Hippocampal place cells that participate more in awake synchronous events are more strongly reactivated during post-experience synchronous events. Awake synchronous neuronal patterns, in cooperation with place-selective firing patterns, determine cell ensembles that undergo pronounced increases and decreases in their correlated spikes. Taken together, awake synchronous events are fundamental for identifying hippocampal neuronal ensembles to be incorporated into synchronous reactivation during subsequent offline states, thereby facilitating memory consolidation.

INTRODUCTION

Learning novel experiences reorganizes the coordinated activity patterns of neuronal ensembles, including changes in their excitability and functional connectivity. The hippocampus has been studied as an appropriate model circuit that undergoes apparent learning-induced changes, which are represented as synchronous reactivation patterns of neuronal ensembles during resting or sleeping after experiencing an environment (termed offline state).[1–6] Post-experience synchronous reactivation coincides with rest/sleep sharp-wave ripples (SWRs) and has been shown to be necessary for the consolidation of initially labile memory.[7–9]

Mechanisms for learning-induced changes in functional neuronal connections can be accounted for by the Hebbian rule; that is, "Neurons that fire together, wire together."[10] When animals move in an environment, hippocampal place cells emit spikes at specific locations (i.e., place fields) that are entrained by theta (6–10 Hz) oscillations.[11] Especially, place cells with overlapping place fields are suitable for generating synchronized spikes within tens of milliseconds and thus more likely to increase their firing associations according to the Hebbian rule.[6] If all place cell pairs with overlapping place fields were equivalently governed by this rule alone, they would undergo similar learning-induced potentiation and thus become more strongly reactivated to similar extents in subsequent offline periods. However, the strength of post-experience synchronous reactivation is not homogeneous across place cells,[12,13] suggesting that neuronal reactivation patterns are not a simple replication of neuronal ensembles encoding an experience.

Another unique hippocampal activity pattern in an environment involves awake synchronous neuronal events, which coincide with awake SWRs and preferentially emerge during nonexploratory consummatory behavior such as reward consumption.[14–17] Recent works have demonstrated that spike trains during awake synchronous events contain reverse and forward replays of past and future behavior on a timescale faster (15–20 times) than a behavioral timescale.[14–19] Awake synchronous events (or replays) also provide specific temporal windows that promote Hebbian plasticity, which is related to the reorganization of functional connection patterns, potentially improving how efficiently animals adapt to new environments[15,20,21] and stabilizing newly formed representations across hippocampal circuits.[17,21] However, the extent to which awake synchronous events contribute to creating neuronal reactivation patterns during post-experience offline states remains unknown.

In this study, we analyzed how hippocampal spike patterns defined by two behavioral states, namely, place cell encoding during running and awake synchronous events, including awake

replays, during consummatory periods in a novel run are incorporated into post-experience synchronous reactivation patterns. We mainly utilized a simple linear track in which animals homogeneously visited all locations on a track during running. The causal roles of awake synchronous events were assessed by selectively disrupting these events using closed-loop electrical manipulations.

RESULTS

Experimental timeline

Rats were trained to perform a U-track run and then implanted with tetrodes. On recording days, the rats first rested in a familiar box, performed the same U-track run (familiar run) for 20 min, rested in the same box (pre-rest) for 60 min, and then performed a novel U-track run on the same-shaped track in a novel room (novel run) for 20 min. As the novel and familiar runs had similar rules, the rats could perform the novel run after running a few laps without prior training. After the novel run, the rat rested in the same box (post-rest) for 60 min (Figure 1A). In the 20-min recording time, the running and reward durations were 6.0 ± 3.0 and 13.4 ± 5.6 min, respectively. A total of 152 CA1 pyramidal neurons were recorded from six rats with no stimulation (Table S1).

To directly evaluate the contributions of reward-associated SWRs, four rats were subjected to an SWR disruption in which closed-loop feedback electrical stimulation with a single pulse (140–180 μA, 100 μs) was applied to the ventral hippocampal commissure upon detection of reward-associated SWRs (SWR disruption).[15,20,21] This stimulation transiently eliminated SWR-associated synchronous spikes (SWR disruption) with a stimulation frequency of 0.21 ± 0.08 Hz (Figure 1B). A total of 135 CA1 pyramidal neurons were recorded from four rats with SWR disruption.

To test whether effects of SWR disruption were specifically due to disruption of synchronous spikes during reward-associated SWRs or due to disruption of the other spike patterns outside SWRs during reward periods, we tested an additional protocol in which stimulation was delivered with a 250-ms delay relative to the SWRs (termed SWR delay). In rats with SWR delay, stimulation frequencies were 0.27 ± 0.07 Hz (Figure 1B) and a total of 101 CA1 pyramidal neurons were recorded from four rats.

Reward-associated synchronous events

Synchronous events in which at least four neurons synchronously emitted spikes within 100 ms were detected in the reward periods (termed reward-associated synchronous events) (Figures S1A, S2A, and S2B). During the reward periods in the novel run, the average frequency of the synchronous events was 0.43 ± 0.17 Hz, which was significantly higher than that in the familiar run (0.29 ± 0.14 Hz; t_5 = 3.66, p = 0.015, paired t test). On average, 14.7% ± 3.8% of spikes during all reward periods were involved in reward-associated synchronous events (n = 6 rats; Figure S1A, left top). Of the 2,169 reward-associated synchronous events that were identified during the novel run, 1,678 (77.4%) events occurred concurrent with awake SWRs (Figure S4A), and 55.8% ± 6.3% of spikes during reward-associated synchronous events corresponded to reward-associated SWRs (Figure S1A, left bottom). Of the 754 reward-associated synchronous events in three rats, 112 (14.9%) events involved awake replay events with temporally compressed (less than 200 ms) sequential place cell firing (Figures S4B and S4C). Unless otherwise specified, we analyzed all awake synchronous events, irrespective of whether they were locked to awake SWRs or composed of awake replays, by assuming that all events had a similar effect on the reorganization of neuronal activity patterns.

We estimated to what extent spikes in reward-associated synchronous events were affected by feedback electrical stimulation during reward. In rats with SWR disruption and SWR delay, the percentages of stimulation periods in entire reward periods were 6.8% ± 1.6% and 5.0% ± 1.9%, respectively (n = 4 rats in each group; Figures S1B and S1C, right). In rats with no stimulation, 17.6% ± 6.3% and 1.9% ± 0.76% of spikes during all reward periods accounted for spikes observed during reward-associated SWRs and during periods 250 ms after the SWRs (corresponding to periods in which delayed stimulation was applied), respectively (n = 6 rats; Figure S1A, right). These results suggest that these fractions of spikes are potentially inhibited by SWR-disruption and SWR-delay protocols. Furthermore, assuming that the effects of stimulation to silence spikes lasted for 200 ms (Figures 1B and S1C) and the frequencies of reward-associated synchronous events and SWRs in naive rats were 0.43 and 0.27 Hz, 8.6% (200 × 0.43/1,000) and 5.4% (200 × 0.27/1,000) of reward-associated synchronous events and SWRs, respectively, were estimated to be inhibited in SWR delay protocols. These influences on synchronous events and SWRs by SWR delay protocols, albeit with a smaller effect compared with direct SWR disruption protocols, possibly explain their substantial effects on post-experience neuronal activity, as described later. The percentages of the number of spikes during all reward-associated synchronous events outside stimulation periods in the total number of spikes in the corresponding periods were 19.3% ± 3.9% and 22.7% ± 6.6% in rats with SWR disruption and SWR delay, respectively (Figures S1B and S1C, left), which were comparable to those observed in the rats with no stimulation (14.7% ± 3.8%), suggesting that neither stimulation protocol prominently affected spike patterns outside the stimulation periods.

The necessity of awake synchronous events in experience-induced reorganization of synchronous reactivation patterns

Similar to the reward periods, synchronous events were detected in the rest periods, which were considered offline synchronous events (Figures S2A and S2B; pre-rest, 0.38 ± 0.19 Hz; post-rest, 0.41 ± 0.21 Hz). Overall, the ratios of theta (6–10 Hz) power to delta (2–4 Hz) power were significantly higher in the pre-rest period than in the post-rest period (Figures S3A and S3B), suggesting higher arousal levels in the pre-rest period. However, the rates of synchronous events did not significantly differ across different theta/delta ratios (Figure S3C). Overall, Pearson correlation coefficients computed from spike patterns in synchronous events between the pre-rest and the post-rest periods were significantly less than 0 (Figures S2C and S2D), suggesting that synchronous spike reactivation patterns during

CellPress
OPEN ACCESS

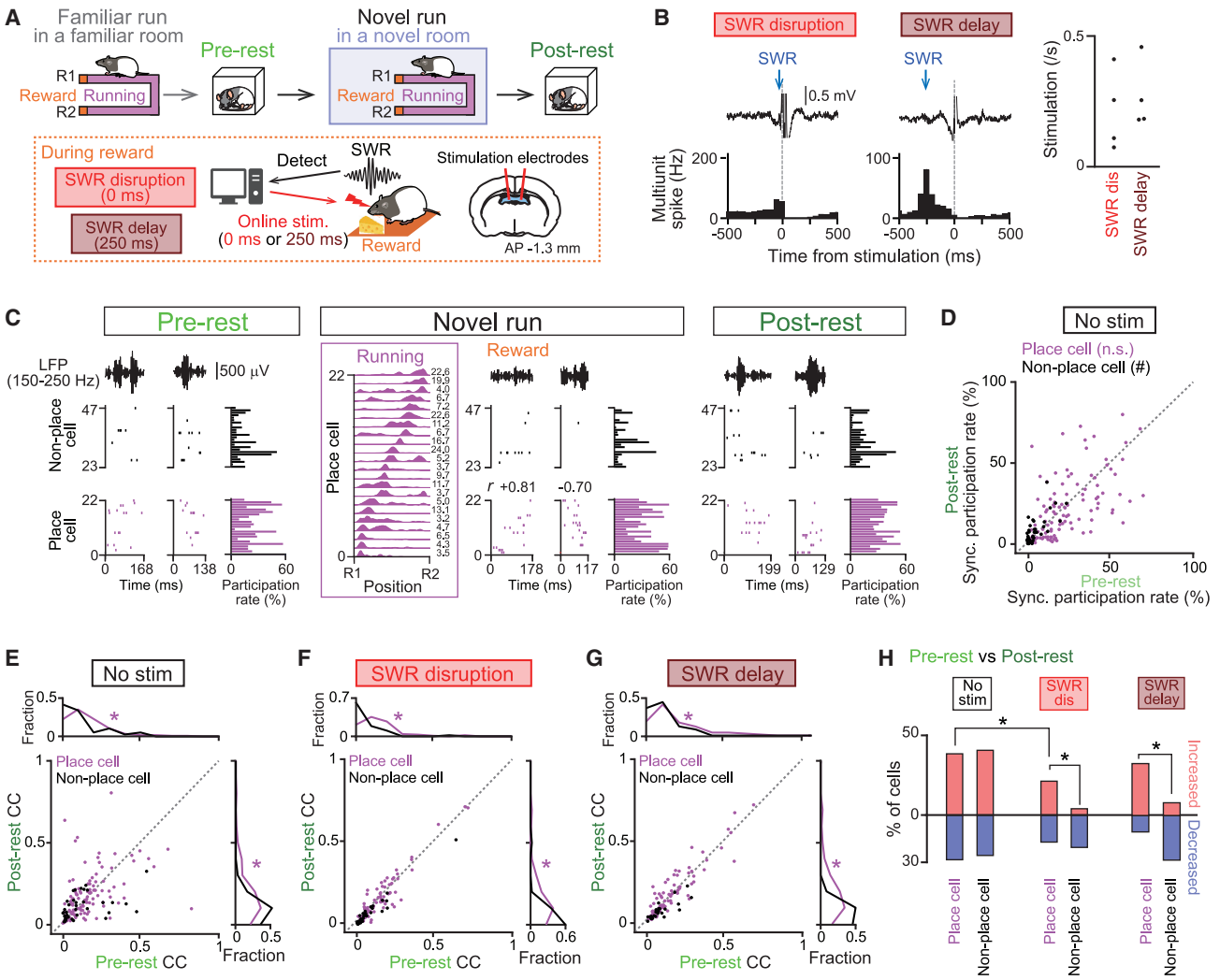

Figure 1. Disruption of reward-associated SWRs eliminates changes in neuronal contributions to post-experience synchronous reactivation patterns

(A) (Top) Experimental timeline. (Bottom) Online closed-loop electrical stimulation was applied to selectively disrupt reward-associated SWRs (SWR disruption). For delayed control, stimulation was delivered with a 250-ms delay relative to detected SWRs (SWR delay). (Right) Stimulation electrodes in the ventral hippocampal commissure.

(B) (Left) Representative local field potential (LFP) traces (top) and multiunit spike rates (bottom) aligned to the time of stimulation in the no-stimulation, SWR-disruption, and 250-ms-delayed control groups. The blue arrows denote the time of SWR detection. (Right) The rate of stimulation during reward periods (n = 4 rats in each group). Each dot represents a rat.

(C) (Top) Ripple band (150–250 Hz)-filtered LFP traces. (Bottom) Raster plots showing spike patterns of place cells (magenta; ordered by their place field locations) and non-place cells (black) (left) and participation rates of individual neurons during synchronous events (right). The sequence scores (*r*) for defining awake replay events during reward periods are shown above.

(D) The participation rates of place (magenta) and non-place (black) cells in synchronous events during the pre- and post-rest periods (place n = 113 cells; non-place n = 39 cells). $^{\#}p < 0.05$.

(E) Cell contributions (CCs) to synchronous events in the pre- and post-rest periods (n = 113 and 39 cells). The top and right histograms show fractions of CCs in the pre- and post-rest periods, respectively. *p < 0.05.

(F) Same as (E), but for rats with SWR disruption (n = 90 and 45 cells; pre-rest, $Z = 5.16$, $*p = 2.4 \times 10^{-7}$; post-rest, $Z = 5.44$, $*p = 5.2 \times 10^{-8}$, Mann-Whitney U test).

(G) Same as (E), but for rats with SWR delay (n = 76 and 25 cells). *p < 0.05.

(H) The proportions of cells showing significant increases and decreases in CCs during the post-rest period compared with those during the pre-rest period (n = 113, 39, 90, 45, 76, and 25 cells). *p < 0.05.

the post-rest period were different than those during the pre-rest period. Similarly, Jaccard correlation coefficients were not significantly different from those of randomized datasets (Figures S2F and S2G). These results suggest that the differences in synchronous events between the pre-rest and the post-rest periods were comparable to random levels.

Furthermore, supervised uniform manifold approximation and projection (UMAP) (Figure S2H) confirmed that the proportion of synchronous events during the pre-rest period assigned to reward (familiar) clusters was significantly higher than that during the post-rest period in the rats with no stimulation (Figure S2I, left), and the proportion of synchronous events during the post-rest period assigned to reward (novel) clusters was significantly higher than that during the pre-rest period (Figure S2I, right). These results demonstrate that synchronous events during the post-rest period were more similar to reward-associated synchronous events during the novel run.

In rats with SWR disruption, both Pearson correlation coefficients and Jaccard similarity coefficients of synchronous events between the pre-rest and the post-rest periods were significantly higher than those observed in rats with no stimulation and those observed in rats with SWR delay (Figures S2D and S2E). Furthermore, the rats with SWR disruption showed Jaccard coefficients that were significantly higher than those observed from the corresponding shuffled datasets (Figures S2F and S2G; SWR disruption). On the other hand, such significant differences were not observed from the rats with no stimulation and SWR delay (Figures S2F and S2G). Taken all together, these results suggest that (1) synchronous neuronal patterns in the post-rest periods were prominently changed from those in the pre-rest periods in rats without SWR disruption and (2) such pronounced changes were eliminated by the disruption of reward-associated SWRs, highlighting the causal role of reward-associated SWRs in the reorganization of post-experience reactivation patterns.

Place cell firing alone does not account for neuronal contributions to post-experience synchronous events

We next asked how individual neurons contribute to changes in synchronous reactivation patterns. In rats with no stimulation, 113 (74.3%) neurons were identified as place cells with at least one place field in the novel run. For each cell, participation rates were computed as the ratio of the number of synchronous events in which the cell showed at least one spike to the total number of synchronous events. The participation rates of place and non-place cells during awake synchronous events were highly heterogeneous, ranging from 0% to 82.1% (19.9% ± 2.0%) and 0% to 75.0% (11.6% ± 2.6%), respectively (Figure 1C). Overall, the participation rates of place cell populations during synchronous events did not differ significantly between the pre-rest and the post-rest periods (Figure 1D; n = 113 cells, $Z = 1.90$, $p = 0.057$, Mann-Whitney U test), whereas non-place cell populations showed significantly lower participation rates during the post-rest period than during the pre-rest period (Figure 1D; n = 39 cells, $Z = 3.00$, $p = 0.0027$, Mann-Whitney U test).

To statistically quantify the contributions of individual neurons to synchronous events, we computed the cell contribution (CC) of each neuron as the difference between the actual average number of activated cells in synchronous events and the average number of activated cells from the corresponding randomized datasets in which interspike intervals were shuffled (Figures 1E and S2J; for more details, see STAR Methods). The CCs of place cells were significantly higher than those of non-place cells in both the pre-rest and the post-rest periods (Figure 1E, top, pre-rest, $Z = 2.42$, $p = 0.032$; right, post-rest, $Z = 2.92$, $p = 0.0072$, Mann-Whitney U test). The proportions of place cells showing significant increases and decreases in their CCs during the post-rest period were 38.9% and 28.3%, respectively, and these proportions were not significantly different from those of non-place cells (Figure 1H; increase, $\chi^2 = 0.053$, $p > 0.99$; decrease, $\chi^2 = 0.10$, $p > 0.99$, chi-squared test followed by Bonferroni correction). These results imply that the presence of place-selective spikes is not a definitive factor for determining change in neuronal contributions to post-experience synchronous reactivation patterns.

The necessity of awake SWRs to changes in the contributions of neurons to post-experience synchronous reactivation

Similar to the rats with no stimulation, the rats with SWR disruption exhibited significantly higher CCs for place cells than for non-place cells in both the pre-rest and the post-rest periods (n = 90 and 45 cells from four rats; Figure 1F, top, pre-rest, $Z = 5.16$, $p = 2.4 \times 10^{-7}$; right, post-rest, $Z = 5.44$, $p = 5.2 \times 10^{-8}$, Mann-Whitney U test). In the rats with SWR disruption, the proportions of place cells showing significant increases and decreases in their CCs were 22.2% and 16.7%, respectively, and the proportion of place cells showing significant increases was significantly smaller than that in the rats with no stimulation (Figure 1H; increase, $\chi^2 = 6.48$, $p = 0.022$, chi-squared test followed by Bonferroni correction; Figure S6).

Neurons that more strongly participate in awake synchronous events show increased contributions to post-experience synchronous reactivation events

The necessity of reward-associated SWRs in experience-induced reorganization implies that neuronal ensembles participating in reward-associated synchronous events are associated with changes in the contributions of individual neurons to post-experience synchronous reactivation events. By statistically comparing the participation rates in reward-associated synchronous events between the familiar and the novel runs (chi-squared test on each neuron, $p < 0.05$), we defined more- and less-participating neurons as neurons showing significantly higher and lower participation rates in the novel run, respectively (Figure 2A, left, labeled in orange and gray; n = 46 and 40 cells). The following statistical comparisons between more- and less-participating neurons were restricted to place cells (Figure 2B; n = 44 and 26 cells). The proportion of more-participating place cells showing significant increases in CCs was 47.7%, which was significantly larger than the proportion showing significant decreases (Figure 2C; indicated by $; $\chi^2 = 4.91$, $p = 0.027$, chi-squared test). Furthermore, the proportion of more-participating place cells showing significant increases was significantly larger than that of less-participating place cells (Figure 2C; $\chi^2 = 5.68$, $p = 0.034$, chi-squared test followed by Bonferroni correction), whereas the proportion of cells showing significant decreases was not significantly different between the two cell groups ($\chi^2 = 1.41$, $p = 0.47$, chi-squared test followed by Bonferroni correction). To further evaluate changes in the neuronal contributions to synchronous reactivation, the difference in the CC between the pre-rest and the post-rest periods (ΔCC) was computed for each neuron. The ΔCCs of more-participating

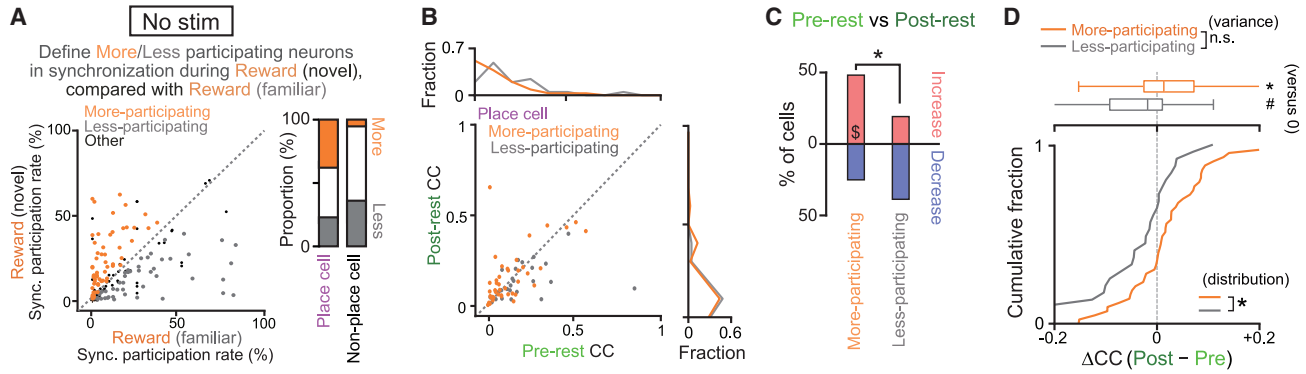

Figure 2. Contribution of neurons involved in reward-associated synchronous events to post-experience synchronous reactivation patterns

(A) For all cells, the participation rates in reward-associated synchronous events in the novel run are plotted against those in the familiar run. More- and less-participating neurons were defined as neurons that had significantly higher and lower participation rates in the novel run compared with in the familiar run, respectively (orange and gray, n = 46 and 40 cells).

(B) The same data shown in Figure 1E but plotted for only place cells with more- (orange) and less- (gray) participating neurons (n = 44 and 26 cells).

(C) The proportions of cells showing significant increases and decreases in CCs in the post-rest period compared with those in the pre-rest period. $^{\$}p < 0.05$, $^{*}p < 0.05$.

(D) Boxplots of ΔCCs (middle, * and # indicate datasets that were significantly greater and less than 0, respectively) and the corresponding cumulative distribution (bottom, n = 44 and 26 neurons; $^{*}p < 0.05$), plotted separately for more- and less-participating neurons. (Top) $F_{43,\ 25} = 0.55$, p = 0.085, *F* test.

place cells were significantly greater than 0 (Figure 2D; boxplot, $Z = 2.35$, p = 0.019, Mann-Whitney U test), whereas the ΔCCs of less-participating place cells were significantly less than 0 ($Z = 2.02$, p = 0.043, Mann-Whitney U test). Moreover, the ΔCCs of more-participating place cells were significantly larger than those of less-participating place cells (Figure 2D; distribution, $Z = 2.55$, p = 0.011, Mann-Whitney U test; variance, $F_{43,\ 25} = 0.55$, p = 0.085, *F* test). Similar statistical results were observed from reward-associated replay events (Figure S4F). Overall, these results suggest that the increased/decreased participation rates of place cells in awake synchronous events during novel experiences are crucial for determining their increased/decreased contributions to post-experience synchronous reactivation.

The necessity of awake SWRs in the reorganization of hippocampal networks

To further examine network-level changes in synchronous reactivation patterns, we measured spike correlations of neuron pairs.[6] A vector was computed for each cell with entries of the number of spikes in each bin (50 ms) in individual synchronous events, and a correlation coefficient of the two vectors was computed. Correlations of cell pairs in which at least one cell participated in fewer than five synchronous events (considered silent cells) were computed as 0. For each rat, the correlation matrices of all cell pairs were constructed (Figure 3A). Cell pairs including non-place cells exhibited significantly lower correlations during the post-rest period (Figure 3B; place-place, n = 1,196 pairs, $Z = 0.52$, p = 0.60; place-non-place, n = 654 pairs, $Z = 2.81$, p = 0.0049; non-place-non-place, n = 169 pairs, $Z = 2.54$, p = 0.011, Mann-Whitney U test).

For further analyses, novel experience-induced changes in spike correlations were computed for each neuron pair as the differences in Fisher's *Z*-transformed correlations from the pre-rest period to the post-rest period (ΔFisher's *Z*) (Figure 3C). The overall ΔFisher's *Z* distributions of cell pairs in rats with no stimulation, SWR disruption, and SWR delay were not significantly different from 0 (Figure 3C–3F; no stimulation, n = 2,018 pairs, $Z = 0.14$, p = 0.89; SWR disruption, n = 2,676 pairs, $Z = 0.034$, p = 0.97; SWR delay, n = 1,310 pairs, $Z = 0.054$, p = 0.97, Mann-Whitney U test versus 0), confirming that the change directions in correlations before and after novel experiences are approximately counterbalanced across place cell networks. The rats with SWR disruption showed significantly smaller variances in their ΔFisher's *Z* distributions compared with the rats with no stimulation (Figure 3F; $F_{2,017,\ 2,675} = 4.29$, p = 6.3×10^{-263}, *F* test followed by Bonferroni correction) and with no SWR delay ($F_{2,017,\ 1,309} = 1.97$, p = 5.5×10^{-39}). These results suggest the necessity of awake SWRs in the experience-induced reorganization of hippocampal networks for further memory consolidation. In addition, the rats with SWR delay showed a variance in the ΔFisher's *Z* distributions that was significantly smaller than that of the rats with no stimulation (Figure 3F; $F_{2,675,\ 1,309} = 0.46$, p = 3.7×10^{-64}, *F* test followed by Bonferroni correction). This result suggests that the substantial disruption of spikes during reward periods outside SWRs in the rats with SWR delay caused an intermediate effect between the rats with no stimulation and those with SWR disruption.

More-participating cells in awake synchronous events show increased spike correlations during post-experience synchronous reactivation

Next, we separately applied the same analyses to more/less-participating place cells (Figures 3G and 3I). More-participating place cell pairs showed significantly higher correlations in the post-rest period than in the pre-rest period (Figure 3H; more-more, n = 216 pairs, $Z = 1.98$, p = 0.048, Mann-Whitney U test). The overall ΔFisher's *Z* distribution of more-participating place cell pairs was significantly higher than those of the other place cell pairs (Figure 3J; more-more versus more-less, n = 216 and

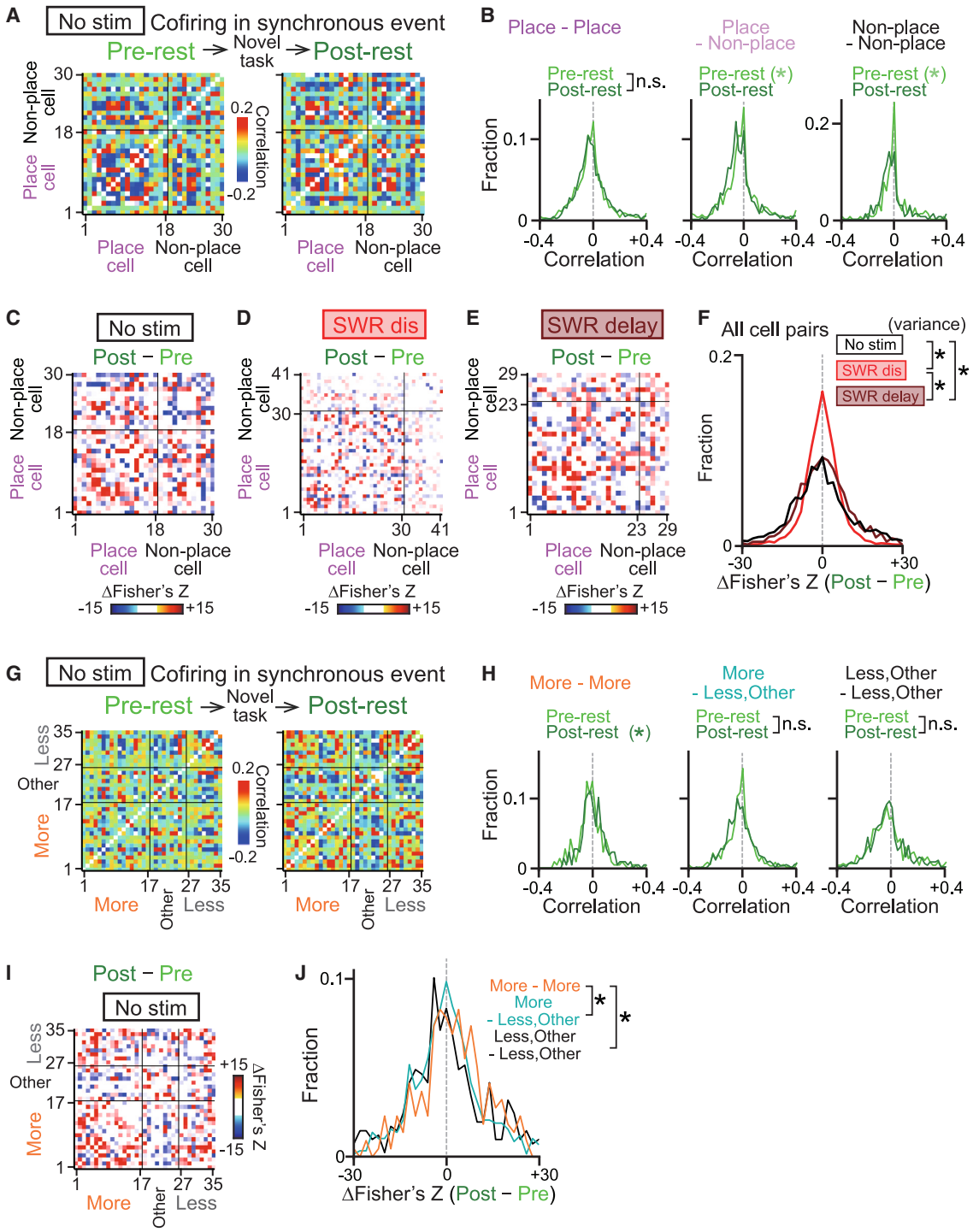

Figure 3. Reward-associated synchronous events are necessary and associated with the reorganization of spiking networks

(A) Correlation matrices for all pairs of neurons computed from synchronous events in the pre- and post-rest periods in a rat.

(B) Distributions of correlations of cell pairs in the pre-rest and post-rest periods (n = 1,196, 654, and 169 pairs). *p < 0.05.

(C) The differences in Fisher's *Z*-transformed correlations between the two rest periods (ΔFisher's *Z*) were computed according to the matrices in (A).

(D) Same as (C), but for a rat with SWR disruption.

(E) Same as (C), but for a rat with SWR delay.

(F) The distributions of ΔFisher's *Z* in rats with no stimulation, SWR disruption, and SWR delay (n = 2,018, 2,676, and 1,310 pairs). *p < 0.05, F-test.

(G) Correlation matrices in a rat with no stimulation. Cells were sorted based on whether they were more- or less-participating cells.

(legend continued on next page)

575 pairs, $Z = 2.61$, p = 0.027; more-more versus less-less, n = 216 and 405 pairs, $Z = 2.83$, p = 0.014; more-less versus less-less, n = 575 and 405 pairs, $Z = 0.82$, p > 0.99, Mann-Whitney U test followed by Bonferroni correction). These results demonstrate that the participation rates of place cell pairs during awake synchronous events determine the changes in their correlated spikes during post-experience synchronous reactivation.

Spatial selectivity and awake synchronous events are associated with increased and decreased spike correlations

We next examined how the post-experience networks were related to combinations of correlated activity during different behavioral periods. For all cell pairs, correlations during running ($correlation_{running}$) on the track were computed with a bin size of 50 ms (Figure 4A, top). Correlations involving cell pairs including at least one cell with a spike rate of less than 0.02 Hz (silent cell) during running were computed as 0. We first investigated how $correlation_{running}$ is related to place-selective firing on the track. Overall, the average $correlation_{running}$ values of close and distant place cell pairs, which were defined as having place field distances of <20 and >60 cm, respectively, were significantly greater and less than 0, respectively (Figure 4B, left; close, n = 404 pairs, $t_{403} = 7.61$, p = 1.9 × 10^{-13}; distant, n = 410 pairs, $t_{409} = 3.38$, p = 7.9 × 10^{-4}, paired t test versus 0), verifying that close and distant place cell pairs are more likely to exhibit positive and negative $correlation_{running}$, respectively. On the other hand, most $correlation_{running}$ of cell pairs including non-place cells was near 0 or less than 0 (Figure 4B, right; place-non-place, n = 652 pairs, $t_{651} = 1.69$, p = 0.092; non-place-non-place, n = 90 pairs, $t_{89} = 0.34$, p = 0.74, paired t test versus 0). Next, correlations during reward-associated synchronous events ($correlation_{reward}$) were computed from all synchronous events in the reward periods (Figure 4A, bottom). The average $correlation_{reward}$ of both close and distant place cell pairs was significantly higher than 0 (Figure 4C, left; close, $t_{403} = 9.72$, p = 3.3 × 10^{-203}; distant, $t_{409} = 3.76$, p = 1.9 × 10^{-4}, t test versus 0), whereas most $correlation_{reward}$ of cell pairs including non-place cells was 0 (including 0 from silent cells) or less than 0 (Figure 4C, right).

We next tested whether different spike correlations during running affect post-experience correlated reactivation (i.e., ΔFisher's Z distributions) (Figures 4D and 4E). Cell pairs with $correlation_{running} > 0$ exhibited significantly higher ΔFisher's Z than cell pairs with $correlation_{running} \leq 0$ (Figure 4E; n = 478 and 1,460 pairs, $Z = 5.49$, p = 3.9 × 10^{-8}, Mann-Whitney U test). Consistently, the proportions of cell pairs with $correlation_{running} > 0$ showing increased and decreased correlations were significantly larger and smaller than those with $correlation_{running} \leq 0$, respectively (Figure 4F; increased, $\chi^2 = 27.44$, p = 3.2 × 10^{-7}; decreased, $\chi^2 = 18.61$, p = 3.2 × 10^{-5}, chi-squared test followed by Bonferroni correction). These results demonstrate that correlated spike patterns during running (i.e., place cells) are associated with post-experience spike activity, which is consistent with the established notion of increased reactivation for experience-related cell ensembles.[2,3,6,22]

Similar to the rats with no stimulation, the rats with SWR disruption showed significantly higher ΔFisher's Z in cell pairs with $correlation_{running} > 0$ compared with those with $correlation_{running} \leq 0$ (Figure 4E; n = 443 and 1,992 pairs, $Z = 3.46$, p = 5.5 × 10^{-4}, Mann-Whitney U test) and significantly larger and smaller proportions of cell pairs showing increased and decreased correlations, respectively, in cell pairs with $correlation_{running} > 0$ compared with those with $correlation_{running} \leq 0$ (Figure 4F; increased, $\chi^2 = 80.78$, p = 0; decreased, $\chi^2 = 6.49$, p = 0.022, chi-squared test followed by Bonferroni correction). Moreover, the proportions of cell pairs with $correlation_{running} \leq 0$ showing increased and decreased correlations in the rats with SWR disruption were significantly smaller than those in rats with no stimulation (Figure 4F; increased, χ^2 = 63.23, p = 7.6 × 10^{-15}; decreased, χ^2 = 104.45, p = 0, chi-squared test followed by Bonferroni correction; Figure S6). These results confirm that reward-associated SWR disruption eliminated experience-induced changes in correlated networks. No significant differences in the proportions of cell pairs showing increased and decreased correlations were observed between the rats with no stimulation and those with SWR delay (Figure 4F; >0: increased, $\chi^2 = 1.32$, p > 0.99; decreased, $\chi^2 = 1.33$, p = 0.99; ≤0: increased, $\chi^2 = 3.24$, p = 0.28; decreased, $\chi^2 = 1.02$, p > 0.99, chi-squared test followed by Bonferroni correction).

Similarly, the relationship between $correlation_{reward}$ and ΔFisher's Z was analyzed (Figure 4G). Cell pairs with $correlation_{reward} > 0$ exhibited significantly higher ΔFisher's Z compared with those with $correlation_{reward} \leq 0$ (Figure 4H; n = 853 and 1,152 pairs, $Z = 3.37$, p = 7.4 × 10^{-4}, Mann-Whitney U test). Consistently, the proportions of cell pairs with $correlation_{reward} > 0$ showing increased and decreased correlations were significantly larger and smaller than those with $correlation_{reward} \leq 0$, respectively (Figure 4I; increased, χ^2 = 28.84, p = 1.5 × 10^{-7}; decreased, χ^2 = 2.89, p = 0.16, chi-squared test followed by Bonferroni correction). These results suggest that positively correlated spikes during reward-associated synchronous events contribute to increased correlated spikes in post-experience reactivation.

Spatial selectivity and awake synchronous events cooperatively determine increased and decreased spike correlations

The $correlation_{reward}$ distributions (Figure 5A) confirmed that cell pairs with positive $correlation_{running}$ exhibited positive $correlation_{reward}$. To examine how combinations of the two correlation patterns were related to post-experience correlated spike patterns, we plotted the $correlation_{running}$ and $correlation_{reward}$ of individual neuron pairs, labeled with different colors according to their ΔFisher's Z value (Figure 5B, left). The joint plot was converted to a color-coded matrix of the average ΔFisher's Z of cell pairs with similar $correlation_{running}$ and $correlation_{reward}$ (bin = 0.1) (Figure 5B, right). Cell pairs with $correlation_{running} > 0$ and $correlation_{reward} > 0.1$ or $correlation_{running} > 0.1$ and

(H) Distributions of correlations of cell pairs in all rats with no stimulation (n = 216, 575, and 405 pairs). *p < 0.05.
(I) The ΔFisher's Z matrix constructed from (G).
(J) The distribution of ΔFisher's Z for cell pairs including more- or less-participating cells. *p < 0.05.

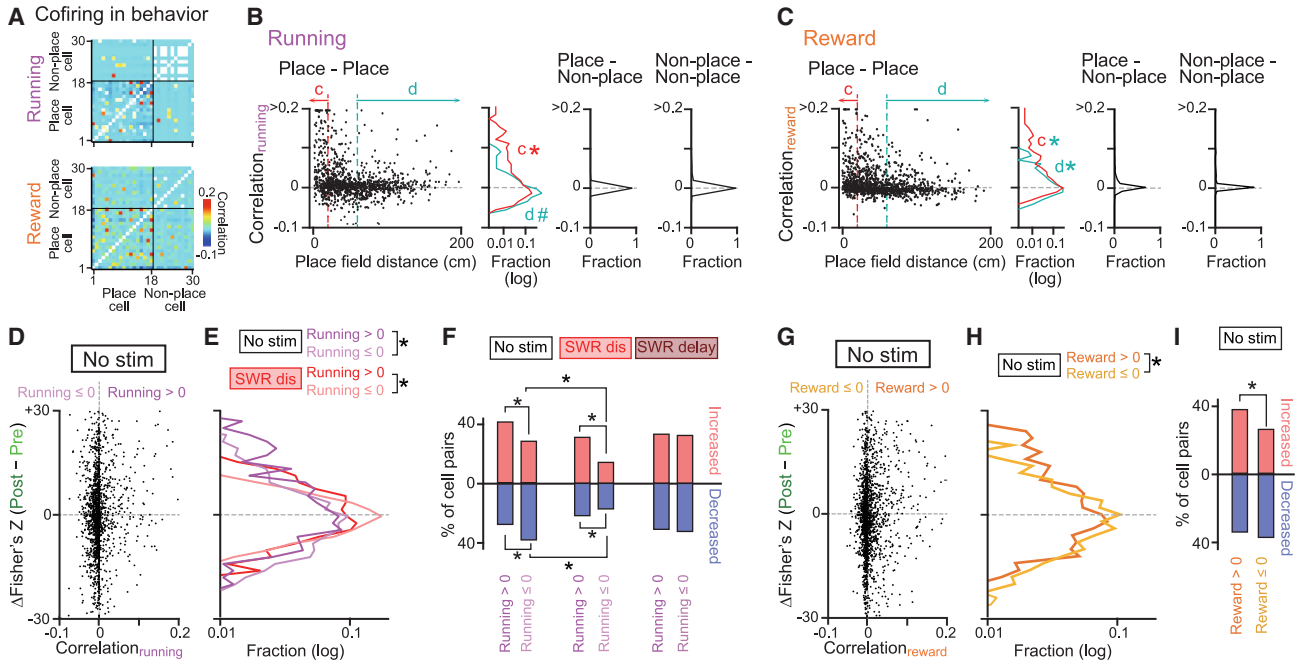

Figure 4. Correlation patterns during running and reward periods are associated with the reorganization of hippocampal networks

(A) Correlation matrices showing all pairs of neurons during all running periods (top) and reward-associated synchronous events (bottom) in a rat.

(B and C) (Left) For all place cell pairs, correlation$_{running}$ (B) and correlation$_{reward}$ (C) were plotted against their place field distance. For visualization, a small jitter was added to the horizontal location on each plot. The next graph shows the distributions for close (c, <20 cm; n = 404) and distant (d, >60 cm; n = 410) place cell pairs. * and # represent that correlations were significantly greater or less than 0, respectively ($p < 0.05$). (Third and fourth graphs) Distributions of correlations including non-place cells (n = 652 and 90 pairs).

(D) For all cell pairs, ΔFisher's *Z* from the pre-rest to the post-rest periods was plotted against correlation$_{running}$ in rats with no stimulation (n = 2,018 pairs).

(E) The distribution of ΔFisher's *Z* for cell pairs with correlation$_{running} > 0$ and correlation$_{running} \leq 0$ in rats with no stimulation and SWR disruption. *$p < 0.05$.

(F) The proportions of cell pairs showing increased and decreased correlations from the pre-rest to the post-rest periods. *$p < 0.05$, chi-squared test followed by Bonferroni correction (detailed statistical values are described in the main text).

(G) For all cell pairs, ΔFisher's *Z* was plotted against correlation$_{reward}$ in rats with no stimulation (n = 2,005 pairs).

(H) The distributions of ΔFisher's *Z* for cell pairs with correlation$_{reward} > 0$ and correlation$_{reward} \leq 0$ in rats with no stimulation (n = 853 and 1,152 pairs). *$p < 0.05$.

(I) The proportions of cell pairs showing increased and decreased correlations from the pre-rest to the post-rest periods. *$p < 0.05$.

correlation$_{reward}$ >0 showed ΔFisher's *Z* that was significantly higher than 0 (Figure 5B; indicated by $; n = 35 pairs, $t_{34} = 2.75$, p = 0.0095; n = 29 pairs, $t_{28} = 2.77$, p = 0.010; n = 25 pairs, $t_{24} = 2.82$, p = 0.0096, paired t test). The proportion of cell pairs showing increased correlations was significantly larger in cell pairs with combinations of correlation$_{running}$ >0 and correlation$_{reward}$ >0 compared with cell pairs with combinations of correlation$_{running}$ >0 and correlation$_{reward}$ ≤0 (Figure 5D; n = 321 and 157 pairs, $\chi^2 = 8.47$, p = 0.022, chi-squared test followed by Bonferroni correction). Furthermore, the proportion of cell pairs showing increased correlations was significantly larger in cell pairs with combinations of correlation$_{running}$ ≤0 and correlation$_{reward}$ >0 compared with cell pairs with combinations of correlation$_{running}$ ≤0 and correlation$_{reward}$ ≤0 (n = 526 and 928 pairs, $\chi^2 = 9.28$, p = 0.014, chi-squared test followed by Bonferroni correction). These results demonstrate that cell pairs with similar correlation$_{running}$ are more likely to increase experience-induced correlated spikes when the cells generate certain levels of positively correlated spikes during reward-associated synchronous events. In contrast, the proportion of cell pairs showing decreased correlations was significantly smaller in cell pairs with combinations of correlation$_{running}$ >0 and correlation$_{reward}$ >0 compared with cell pairs with combinations of correlation$_{running}$ ≤0 and correlation$_{reward}$ >0 ($\chi^2 = 8.43$, p = 0.022, chi-squared test followed by Bonferroni correction) and cell pairs with combinations of correlation$_{running}$ ≤0 and correlation$_{reward}$ ≤0 ($\chi^2 = 13.55$, p = 0.0014, chi-squared test followed by Bonferroni correction). In addition, the proportion of cell pairs showing decreased correlations was significantly smaller in cell pairs with combinations of correlation$_{running}$ >0 and correlation$_{reward}$ ≤0 compared with cell pairs with combinations of correlation$_{running}$ ≤0 and correlation$_{reward}$ ≤0 ($\chi^2 = 7.97$, p = 0.029, chi-squared test followed by Bonferroni correction).

We finally examined whether post-experience changes in correlated spikes could be explained by place-selective firing patterns and correlation$_{running}$. Similar to Figure 5B, we constructed color-coded matrices of the average ΔFisher's *Z* for place cell pairs with different place field distances and correlation$_{reward}$ values (Figure 5E, left; n = 1,144 pairs). Only place cell pairs with field distances <50 cm and correlation$_{reward}$ >0.1 showed ΔFisher's *Z* that was significantly higher than 0 (Figure 5E; indicated by $; n = 53 pairs, $t_{52} = 3.90$, p = 2.8 × 10^{-4},

CellPress
OPEN ACCESS

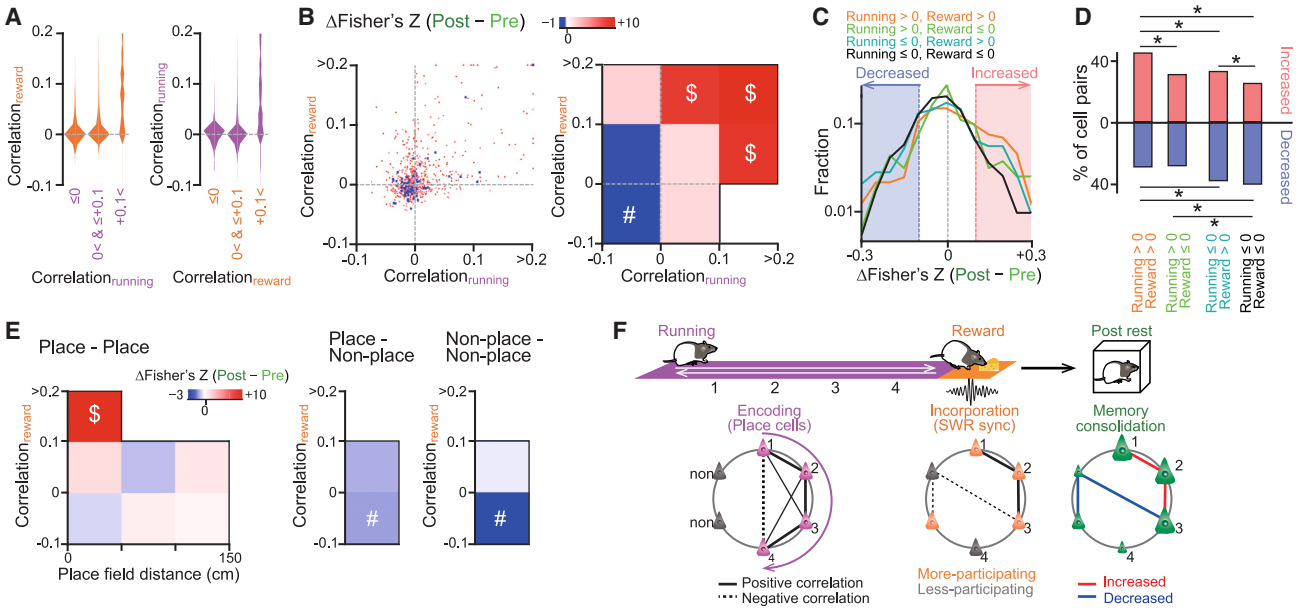

Figure 5. Cooperative correlation patterns during running and reward periods lead to the reorganization of hippocampal networks

(A) Correlation$_{reward}$ distributions with different correlation$_{running}$ (left; n = 1,455, 422, and 56 pairs), and correlation$_{running}$ distributions with different correlation$_{reward}$ (right; n = 1,086, 776, and 71 pairs).

(B) (Left) Plot of correlation$_{running}$ and correlation$_{reward}$ for all cell pairs, which are labeled by different colors depending on their ΔFisher's *Z*. Each dot represents a cell pair (n = 1,932 pairs). (Right) The corresponding color-coded matrix shows the average ΔFisher's *Z* of all cell pairs involved in each combination of correlation$_{running}$ and correlation$_{reward}$ with a bin of 0.1. Bins with fewer than four plots were excluded. $ and # indicate bins with datasets that were significantly greater and less than 0, respectively.

(C) The ΔFisher's *Z* distributions of all cell pairs with different combinations of correlation$_{running}$ and correlation$_{reward}$ (n = 321, 157, 526, and 928 pairs).

(D) According to (C), the proportions of cell pairs with increased and decreased correlations were computed. *p < 0.05, chi-squared test followed by Bonferroni correction (detailed statistical values are described in the main text).

(E) (Left) A color-coded matrix showing the average ΔFisher's *Z* of all place cell pairs with different combinations of place field distances and correlation$_{reward}$. $ indicates a bin with datasets that were significantly greater than 0 (n = 53 pairs), $^{\$}p < 0.05$. (Middle and right) Color-coded matrices showing average ΔFisher's *Z* for cell pairs including non-place cells with different correlation$_{reward}$ values. # indicates a bin with datasets that were significantly less than 0 ($^{\#}p < 0.05$).

(F) Schematic illustration. Four place cells are ordered according to the locations of their place fields. In addition, two non-place cells are shown (non). In the running and reward periods, the colored neurons indicate active neurons, and the solid and dotted black lines represent synchronous and asynchronous neuron pairs, respectively. In the post-rest period, the size of the neurons represents changes in their contribution to synchronous reactivation, and the red and blue lines represent cell pairs with increased and decreased correlations, respectively.

paired t test), suggesting that similar spatial firing patterns during running and correlated spikes during awake synchronous events are both necessary for inducing increased spike correlations. On the other hand, place-non-place cell pairs and non-place cell pairs with correlation$_{reward}$ ≤0 showed ΔFisher's *Z* that was significantly lower than 0 (Figure 5E; indicated by #; middle, n = 306 pairs, t_{305} = 2.00, p = 0.046; right, n = 153 pairs, t_{49} = 3.55, p = 8.7 × 10^{-4}, paired t test). These results suggest that cell pairs, including non-place cells that do not generate synchronous spikes during awake synchronous events, are more likely to decrease spike correlations after novel experiences.

Overall, we propose a scheme that explains experience-induced reorganization in hippocampal circuits (Figure 5F): place cell networks involved in awake synchronous events specifically increase their contributions and correlated spikes in post-experience synchronous reactivation events, thereby facilitating memory consolidation. Moreover, non-place cell ensembles that are not associated with awake synchronous events decrease their post-experience correlated spikes. Overall, the proportions of cell pairs with increased and decreased correlated spikes are essentially counterbalanced.

Similar results are observed from a spatial learning task

We further examined whether similar results would be obtained from a spatial learning task (Figure 6A; for more detail, see Igata et al.[15]). Neurons that specifically encoded pre-existing information (path S-C_1-G-S) in the pre-learning phase and novel information (path S-C_2-G) in the learning phase were classified as "new" and "old" cells, respectively (Figure 6B). Awake synchronous events were detected when the rats stopped at S, C_1, C_2, and G (Figure 6C). Similar to the definitions used in Figure 2A, more- and less-participating neurons were statistically defined (Figures 6D and 6E; n = 160 and 102 cells). The proportion of more-participating cells showing significant increases in CCs during the post-rest period compared with those during the pre-rest period was significantly larger than that of less-participating cells (Figure 6F; χ^2 = 9.51, p = 0.0020), and the ΔCCs of more-participating cells were significantly higher than those of less-participating cells (distribution, *Z* = 4.57, p = 4.9 × 10^{-6},

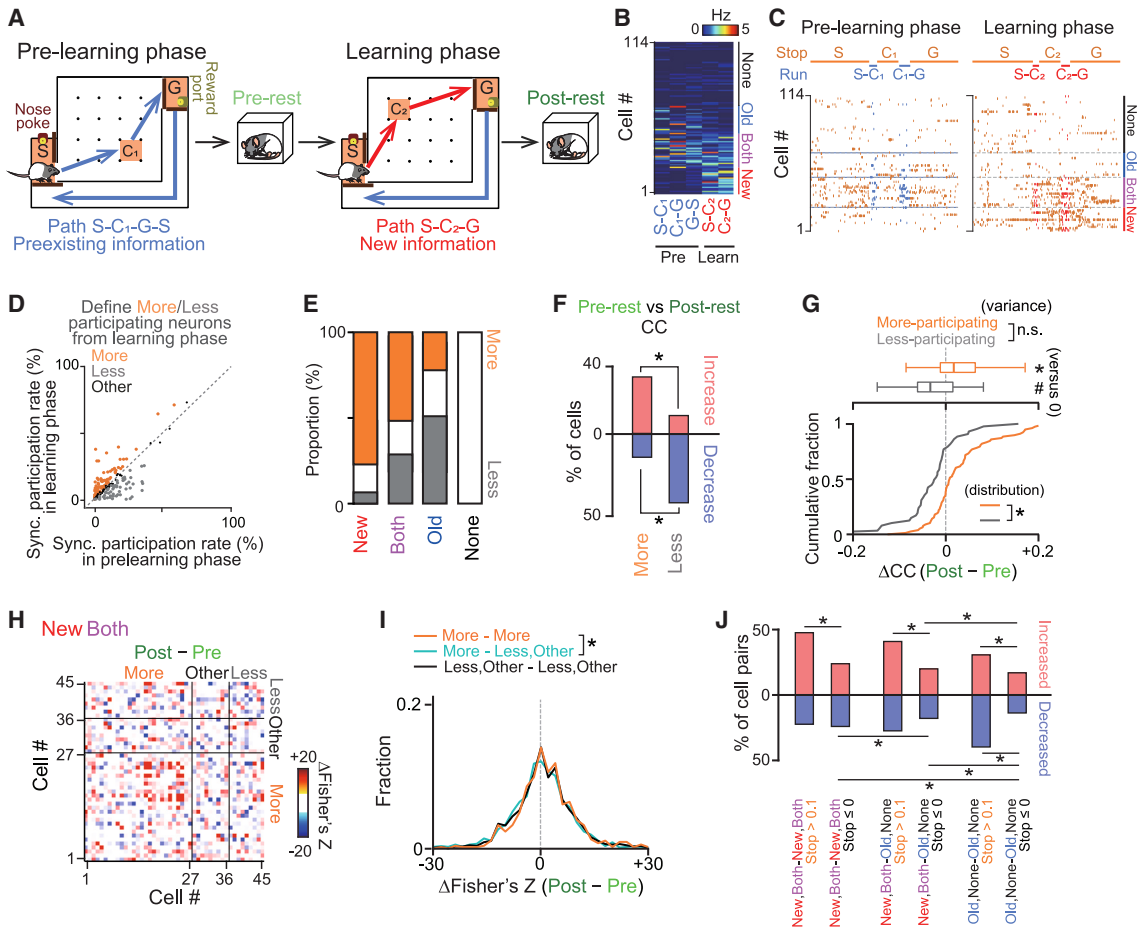

Figure 6. Similar associations between awake synchronous events and post-experience reactivation are observed from a spatial learning task

(A) Experimental timeline of a spatial learning task.

(B) Firing rates of individual neurons in each path.

(C) Animal locations and a raster plot of the spike patterns of 114 neurons. Synchronous events were detected in the S, C_1, G, and C_2 areas.

(D and E) More- and less-participating neurons were defined (orange and gray, n = 160 and 102 cells).

(F) The proportions of cells showing significant increases and decreases in CCs during the post-rest period. *p < 0.05.

(G) Differences in CCs between the pre- and the post-rest periods (* and # indicate datasets significantly higher and lower than 0, respectively; n = 79 and 44 cells; *p < 0.05) and the corresponding cumulative distributions (Z = 4.57, *p = 4.9 × 10^{-6}, Mann-Whitney U test). (Top) $F_{78, 43}$ = 1.10, p = 0.73, F test.

(H) The ΔFisher's Z matrix between the pre-rest and the post-rest periods.

(I) The distributions of ΔFisher's Z for cell pairs classified as more- and less-participating cells (n = 548, 927, and 1,149 pairs). *p < 0.05.

(J) The proportions of cell pairs with increased and decreased correlations. *p < 0.05, chi-squared test followed by Bonferroni correction.

Mann-Whitney U test; variance, $F_{66, 23}$ = 0.74, p = 0.34, F test). In correlation analyses (Figure 6H), more-participating cell pairs showed ΔFisher's Z distributions that were significantly higher than those of cell pairs including less-participating cells (Figure 6I; n = 548 pairs, Z = 2.91, p = 0.011, Mann-Whitney U test followed by Bonferroni correction). The proportions of cell pairs showing increased correlations of spikes during stop periods ($correlation_{stop}$) were significantly higher in all cell pair types with $correlation_{stop}$ >0.1, compared with those with $correlation_{stop}$ ≤0 (Figure 6J; within new,both-new,both, χ^2 = 16.04, p = 1.8 × 10^{-4}; within new,both-old,none, χ^2 = 11.54, p = 0.0041; within old,none-old,none, χ^2 = 6.78, p = 0.028, chi-squared test followed by Bonferroni correction). Overall, the spatial learning task results support that new information-encoding cell ensembles increase their contributions during post-experience synchronous reactivation events specifically when the cells are associated with awake synchronous events during novel learning.

DISCUSSION

It has been well established that hippocampal cell ensembles that encode spatial experiences are more preferentially reactivated during subsequent offline synchronous events.[1–5,22–25] Importantly, post-experience reactivation patterns are dominated by default pre-configured networks that are represented

during pre-experience periods.[26,27] In this scheme, subsets of place cells that are newly created during novel experiences are incorporated into the pre-existing networks.[28,29] Our results confirmed similarities in the participation rates of individual neurons and the coactivation patterns of cell pairs in synchronous events between the pre-rest and the post-rest periods. Based on these observations, we quantified changes in spike patterns during post-experience synchronous events in reference to those observed during pre-experience events. These compensations allowed us to more accurately identify heterogeneous changes in synchronous reactivation patterns across neuronal ensembles in the post-rest period, which are associated with neuronal ensembles that are related to awake synchronous events rather than only experience-encoding cell ensembles (e.g., place cells).

Our claims are not contradictory to the established view of post-experience place cell reactivation.[3,6] In fact, we confirmed that a certain subset of place cells with overlapping place fields showed stronger correlations in post-experience synchronous reactivation events. In addition to this established scheme, we highlighted the necessity of awake synchronous events for triggering sufficient changes in neuronal ensembles. O'Neil et al.[6] has demonstrated that place cell pairs with different place fields and asynchronous spikes in a two-dimensional open field weaken their cofiring in post-experience reactivation. We confirmed that neuron pairs, including those with non-place cells showing negative spike correlations during reward-associated synchronous events, showed decreased spike correlations in post-experience synchronous reactivation events. Taken together, awake synchronous events and spatial firing patterns are both crucial factors in the bidirectional modulation of neuronal functional connectivity in post-experience neuronal reactivation. These results verify that spike synchrony between two neurons within narrow temporal (tens of milliseconds) windows during consummatory periods enhances their correlational activity, which is consistent with a form of Hebbian learning known as spike timing-dependent plasticity,[30] whereas spike asynchrony, in which one neuron is active while the other neuron is silent, results in decreased correlational activity. In nature, animals spend more time performing consummatory behaviors than performing exploratory and running behaviors in environments. Following the Hebbian rule, in which the number of times that neurons fire together is a robust predictor of strengthened functional connections,[6,10] correlated activity during longer consummatory periods may have a stronger influence on overall experience-induced changes in hippocampal networks than correlated activity during shorter running periods.

Our results suggest that the directions of learning-induced changes in neuronal activity patterns during post-experience synchronous reactivation are essentially counterbalanced. Roux et al.[21] demonstrated that optogenetic inhibition of awake SWRs during learning tasks did not affect overall changes in participation rates of place cells between pre-experience and post-experience slow-wave sleep periods. Our results are in accordance with this study, demonstrating that rats with SWR disruption and rats with no stimulation showed no significant differences in terms of the total contributions of their place cell populations to synchronous events between pre-experience and post-experience offline states. In addition, we revealed that awake SWRs are crucial in amplifying experience-induced changes, increasing the proportions of neurons showing both learning-dependent pronounced increases and decreases in their contributions and spike correlations during post-experience synchronous reactivation events.

Our study suggests that awake synchronous events are fundamental for identifying which neuronal ensembles encoding experiences are reactivated and correlated to create novel reactivation patterns during memory consolidation. The new roles of awake synchronous events add to a growing body of evidence that awake SWRs and replays are essential for stabilizing spatial maps and planning and optimizing behavioral strategies.[15,19–21,31] Two distinct types of behavior-related spike patterns in the hippocampus, namely, experience-encoding spikes (e.g., place-selective firing) and awake synchronous events, cooperatively trigger the bidirectional modulation of functional connections in hippocampal circuits to efficiently create and maintain novel memories.

Limitation of the study

We observed that stimulation in SWR delay protocols partly affected post-experience neuronal activity patterns, while they were smaller than those observed from SWR disruption. On the other hand, early works have reported that similar SWR delay protocols had no prominent effects at behavioral levels.[15,20] It remains to be determined how these differences in the effects of SWR delay protocols are reconciled. A possible explanation is that spike patterns that are retained in SWR delay protocols are sufficient to induce proper behavior. Another explanation might be that initial transient large-scale synchronous depolarization induced by the artificial stimulation, which is followed by a global suppression of neuronal spikes, caused substantial changes observed in the SWR delay group. In addition, recent works have demonstrated that awake synchronous events contain spike sequences of reverse and forward replays of behavior.[15,17,20,21] In this study, due to the limitation of spike samples, our spike analysis did not analyze such fine orders of spikes at millisecond timescales.

STAR★METHODS

Detailed methods are provided in the online version of this paper and include the following:

- KEY RESOURCES TABLE
- RESOURCE AVAILABILITY
  - Lead contact
  - Materials availability
  - Data and code availability
- EXPERIMENTAL MODEL AND STUDY PARTICIPANT DETAILS
- METHOD DETAILS
  - Behavioral training for a U track run
  - Surgical procedures
  - Adjusting electrode depth
  - Electrophysiological recording
  - Recordings from a novel run

- SWR disruption by closed-loop electrical stimulation
- Histological analysis to confirm tetrode locations
- A spatial learning task

- QUANTIFICATION AND STATISTICAL ANALYSIS
  - Definition of behavioral periods in the U track run
  - Definition of behavioral periods in the spatial learning task
  - Spike sorting of hippocampal neurons
  - Spatial firing patterns
  - Detection of synchronous events and SWRs
  - Definition of replay events
  - Similarity of synchronous events
  - Uniform manifold approximation and projection (UMAP)
  - Per-cell contribution to synchronous events (CC)
  - Definition of more/less-participating neurons
  - Spike correlations in a cell pair
  - Statistical analysis

SUPPLEMENTAL INFORMATION

Supplemental information can be found online at https://doi.org/10.1016/j.celrep.2023.112871.

ACKNOWLEDGMENTS

This work was supported by KAKENHI (20H03545, 21H05243) from the Japan Society for the Promotion of Science (JSPS), grants (JP21zf0127004) from the Japan Agency for Medical Research and Development, grants from the Japan Science and Technology Agency (JST) (JPMJCR21P1, JPMJMS2292), the Uehara Memorial Foundation, and Research Foundation for Opto-Science and Technology to T.S.; grants from the JST Exploratory Research for Advanced Technology (JPMJER1801) and Institute for AI and Beyond of the University of Tokyo to Y.I.; and JSPS Research Fellowships to S.Y. and H.I.

AUTHOR CONTRIBUTIONS

S.Y. and T.S. designed the study. S.Y. and H.I. acquired the electrophysiological data from U-track and spatial learning task, respectively, and performed spike sorting. S.Y. and T.S. performed the analyses and prepared the figures. T.S. wrote the main manuscript text. Y.I. supervised the project, and all the authors reviewed the main manuscript text.

DECLARATION OF INTERESTS

The authors declare no competing interests.

INCLUSION AND DIVERSITY

We support inclusive, diverse, and equitable conduct of research.

Received: April 21, 2023
Revised: May 30, 2023
Accepted: July 11, 2023
Published: July 25, 2023

REFERENCES

1. Buzsáki, G. (2015). Hippocampal sharp wave-ripple: A cognitive biomarker for episodic memory and planning. Hippocampus *25*, 1073–1188.
2. Kudrimoti, H.S., Barnes, C.A., and McNaughton, B.L. (1999). Reactivation of hippocampal cell assemblies: effects of behavioral state, experience, and EEG dynamics. J. Neurosci. *19*, 4090–4101.
3. Wilson, M.A., and McNaughton, B.L. (1994). Reactivation of hippocampal ensemble memories during sleep. Science *265*, 676–679.
4. Giri, B., Miyawaki, H., Mizuseki, K., Cheng, S., and Diba, K. (2019). Hippocampal Reactivation Extends for Several Hours Following Novel Experience. J. Neurosci. *39*, 866–875.
5. Csicsvari, J., Hirase, H., Mamiya, A., and Buzsáki, G. (2000). Ensemble patterns of hippocampal CA3-CA1 neurons during sharp wave-associated population events. Neuron *28*, 585–594.
6. O'Neill, J., Senior, T.J., Allen, K., Huxter, J.R., and Csicsvari, J. (2008). Reactivation of experience-dependent cell assembly patterns in the hippocampus. Nat. Neurosci. *11*, 209–215.
7. Girardeau, G., Benchenane, K., Wiener, S.I., Buzsáki, G., and Zugaro, M.B. (2009). Selective suppression of hippocampal ripples impairs spatial memory. Nat. Neurosci. *12*, 1222–1223.
8. Gridchyn, I., Schoenenberger, P., O'Neill, J., and Csicsvari, J. (2020). Assembly-Specific Disruption of Hippocampal Replay Leads to Selective Memory Deficit. Neuron *106*, 291–300.e6.
9. van de Ven, G.M., Trouche, S., McNamara, C.G., Allen, K., and Dupret, D. (2016). Hippocampal Offline Reactivation Consolidates Recently Formed Cell Assembly Patterns during Sharp Wave-Ripples. Neuron *92*, 968–974.
10. Hebb, D.O. (1949). The Organization of Behavior; a Neuropsychological Theory (Wiley).
11. O'Keefe, J., and Nadel, L. (1978). The Hippocampus as a Cognitive Map (Oxford University Press).
12. Mizuseki, K., and Buzsáki, G. (2013). Preconfigured, skewed distribution of firing rates in the hippocampus and entorhinal cortex. Cell Rep. *4*, 1010–1021.
13. Ylinen, A., Bragin, A., Nádasdy, Z., Jandó, G., Szabó, I., Sik, A., and Buzsáki, G. (1995). Sharp wave-associated high-frequency oscillation (200 Hz) in the intact hippocampus: network and intracellular mechanisms. J. Neurosci. *15*, 30–46.
14. Singer, A.C., and Frank, L.M. (2009). Rewarded outcomes enhance reactivation of experience in the hippocampus. Neuron *64*, 910–921.
15. Igata, H., Ikegaya, Y., and Sasaki, T. (2021). Prioritized experience replays on a hippocampal predictive map for learning. Proc. Natl. Acad. Sci. USA *118*, e2011266118.
16. Ambrose, R.E., Pfeiffer, B.E., and Foster, D.J. (2016). Reverse Replay of Hippocampal Place Cells Is Uniquely Modulated by Changing Reward. Neuron *91*, 1124–1136.
17. Dupret, D., O'Neill, J., Pleydell-Bouverie, B., and Csicsvari, J. (2010). The reorganization and reactivation of hippocampal maps predict spatial memory performance. Nat. Neurosci. *13*, 995–1002.
18. Foster, D.J., and Wilson, M.A. (2006). Reverse replay of behavioural sequences in hippocampal place cells during the awake state. Nature *440*, 680–683.
19. Pfeiffer, B.E., and Foster, D.J. (2013). Hippocampal place-cell sequences depict future paths to remembered goals. Nature *497*, 74–79.
20. Jadhav, S.P., Kemere, C., German, P.W., and Frank, L.M. (2012). Awake hippocampal sharp-wave ripples support spatial memory. Science *336*, 1454–1458.
21. Roux, L., Hu, B., Eichler, R., Stark, E., and Buzsáki, G. (2017). Sharp wave ripples during learning stabilize the hippocampal spatial map. Nat. Neurosci. *20*, 845–853.
22. Lee, A.K., and Wilson, M.A. (2002). Memory of sequential experience in the hippocampus during slow wave sleep. Neuron *36*, 1183–1194.
23. Nishimura, Y., Ikegaya, Y., and Sasaki, T. (2021). Prefrontal synaptic activation during hippocampal memory reactivation. Cell Rep. *34*, 108885.
24. Skaggs, W.E., and McNaughton, B.L. (1996). Replay of neuronal firing sequences in rat hippocampus during sleep following spatial experience. Science *271*, 1870–1873.

25. Silva, D., Feng, T., and Foster, D.J. (2015). Trajectory events across hippocampal place cells require previous experience. Nat. Neurosci. *18*, 1772–1779.

26. Dragoi, G., and Tonegawa, S. (2011). Preplay of future place cell sequences by hippocampal cellular assemblies. Nature *469*, 397–401.

27. Liu, K., Sibille, J., and Dragoi, G. (2018). Generative Predictive Codes by Multiplexed Hippocampal Neuronal Tuplets. Neuron *99*, 1329–1341.e6.

28. Liu, K., Sibille, J., and Dragoi, G. (2019). Preconfigured patterns are the primary driver of offline multi-neuronal sequence replay. Hippocampus *29*, 275–283.

29. Grosmark, A.D., and Buzsáki, G. (2016). Diversity in neural firing dynamics supports both rigid and learned hippocampal sequences. Science *351*, 1440–1443.

30. Wittenberg, G.M., and Wang, S.S.H. (2006). Malleability of spike-timing-dependent plasticity at the CA3-CA1 synapse. J. Neurosci. *26*, 6610–6617.

31. Ólafsdóttir, H.F., Barry, C., Saleem, A.B., Hassabis, D., and Spiers, H.J. (2015). Hippocampal place cells construct reward related sequences through unexplored space. Elife *4*, e06063.

32. Yagi, S., Igata, H., Shikano, Y., Aoki, Y., Sasaki, T., and Ikegaya, Y. (2018). Time-varying synchronous cell ensembles during consummatory periods correlate with variable numbers of place cell spikes. Hippocampus *28*, 471–483.

33. Aoki, Y., Igata, H., Ikegaya, Y., and Sasaki, T. (2019). The Integration of Goal-Directed Signals onto Spatial Maps of Hippocampal Place Cells. Cell Rep. *27*, 1516–1527.e5.

34. Schmitzer-Torbert, N., Jackson, J., Henze, D., Harris, K., and Redish, A.D. (2005). Quantitative measures of cluster quality for use in extracellular recordings. Neuroscience *131*, 1–11.

35. Wu, X., and Foster, D.J. (2014). Hippocampal replay captures the unique topological structure of a novel environment. J. Neurosci. *34*, 6459–6469.

STAR★METHODS

KEY RESOURCES TABLE

REAGENT or RESOURCE	SOURCE	IDENTIFIER
Chemicals, peptides, and recombinant proteins		
Isoflurane	Zoetis	Cat#6073253
Praformaldehyde	Nacalai tesque	Cat#M8E4590
Cresyl violet	Sigma-Aldrich	Cat#125K3707
Re-fine Bright	Yamahachi Dental Mfg., Co.	Cat#KH01
Hydrogen Hexachloroplatinate(IV) Hexahydrate	Nacalai tesque	Cat#V8P4386
Deposited data		
Behavior and spike data	Mendeley Data	https://doi.org/10.17632/svhr62dxx3.1 https://doi.org/10.17632/4xk5w69yr5.1
Sprague Dawley rat	Japan SLC	slc:SD
Software and algorithms		
MATLAB R 2022a	MathWorks	https://jp.mathworks.com/
MClust	A.D. Redish	http://redishlab.neuroscience.umn.edu/MClust/MClust.html
Python 2.7	Python Software Foundation	https://www.python.org/about/
Other		
Platinum-Iridium tetrode wire	California Fine Wire Company	Cat#CFW0011173
Stimulation electrode	Unique medical	TOG217-049
Microdrive	Custom built	N/A
Micro syringe	Ito	Model: MS-E05
Syringe pump	Muromachi	Model: Legato 100
Cannula	Eicom	Model: AC-5, AG-12, AD-12
Microtome	Leica	Model: SM2010 R
Neural signal processor	BLACKROCK	Model: Cerebus
Single channel pulse generator	WPI	A310

RESOURCE AVAILABILITY

Lead contact

Further information and requests for resources and reagents should be directed to and will be fulfilled by the lead contact, Takuya Sasaki (takuya.sasaki.b4@tohoku.ac.jp).

Materials availability

This study did not generate any unique reagents. The CAD files for creating the feeding wheel and feeding port by 3D printers are available from the lead contact upon request.

Data and code availability

- The original data are provided on Mendeley Data (https://doi.org/10.17632/svhr62dxx3.1). To reduce the number of animals, confirm the reproducibility of our study, we analyzed additional datasets from Igata et al. (2021), which have been available at Mendeley data (https://doi.org/10.17632/4xk5w69yr5.1).
- Code necessary to reproduce the Matlab-generated figures in this study are provided and maintained at Mendeley data (https://doi.org/10.17632/svhr62dxx3.1)
- Any additional information required to reanalyze the data reported in this work paper is available from the lead contact upon request.

EXPERIMENTAL MODEL AND STUDY PARTICIPANT DETAILS

All experiments were performed with the approval of the experimental animal ethics committee at the University of Tokyo (approval number: P29-7) and according to the NIH guidelines for the care and use of animals. For the U track run, a total of 14 male Long Evans rats (3–6 months old) with preoperative weights of 380–500 g were used in this study. The animals were housed individually and maintained on a 12-h light/12-h dark schedule with lights off at 7:00 AM. All the animal subjects were purchased from SLC (Shizuoka, Japan). Following at least 1 week of laboratory adaptation, the rats were reduced to 85% of their *ad libitum* weight by limiting daily feeding. Water was readily available. As only male rats were used in this study, we cannot determine whether the same data are obtained from female rats.

METHOD DETAILS

Behavioral training for a U track run

Before surgery, the rat was trained daily to perform a U-shaped track run in a familiar room. On one training day, the rat was trained to run back and forth on a U-shaped track consisting of two 100 × 9 cm^2 peripheral alleyways and one 50 × 9 cm^2 central alleyways (90 cm elevated from the floor) to obtain a constant amount of ~0.2 ml of chocolate milk reward placed at the track end. This training was repeated daily for 20–40 min for at least a total of 9 times before and after surgery. The rat was maintained in a rest box (30 × 30 cm^2) outside the track before and after the run.

Surgical procedures

For the U track run, six and eight rats underwent surgery to implant recording electrodes only and a combination of recording and stimulating electrodes, respectively. Briefly, the rats were anesthetized with isoflurane gas (0.5–2.5%), and a 2-cm midline incision was made from the area between the eyes to the cerebellum. For all rats, a craniotomy with a diameter of 0.9–1.6 mm was created above the right dorsal hippocampus (3.8 mm posterior and 2.7 mm lateral to bregma) using a high-speed drill, and the dura was surgically removed. Two stainless-steel screws were implanted in the bone above the prefrontal cortex to serve as ground electrodes. Using a 3D printer (Form 2, Formlabs) an electrode assembly consisting of 8–16 independently movable tetrodes was created and stereotaxically implanted above the craniotomy[15,32,33]. The tips of the tetrode bundles were lowered to the cortical surface, and the electrodes were inserted 1.0 mm into the brain at the end of the surgery. The electrodes were constructed from 17-μm-wide polyimide-coated platinum-iridium (90/10%) wire (California Fine Wire California Fine Wire Co., Grover Beach, CA), and the electrode tips were plated with platinum to reduce their electrode impedances to 150–300 kΩ at 1 kHz. For eight rats, craniotomies (1.3 mm posterior and 1.7 mm lateral to the bregma) with a diameter of ~1 mm were additionally created using a high-speed drill, and stainless bipolar electrodes were implanted at a depth of 3.7 mm at an angle of 6.9° into the right side or both sides of the ventral hippocampal commissure (vHC)[15].

All the recording devices were secured to the skull using stainless-steel screws and dental cement. Following surgery, each rat was housed individually in transparent Plexiglass with free access to water and food for at least 5 days and was then food-deprived until they reached 85% of their previous body weight.

Adjusting electrode depth

Each rat was connected to the recording equipment via a Cereplex M (Blackrock) digitally programmable amplifier, close to the rat's head. The output of the headstage was connected via a lightweight multiwire tether and a commutator to a Cerebus recording system (Blackrock), a data acquisition system. Electrode turning was performed while the rat was resting in a pot placed on a pedestal. The electrode tips were slowly advanced by 25–100 μm per day for 16–25 days until spiking cells were encountered in the CA1 layer of the hippocampus, which was identified on the basis of local field potential (LFP) signals and single-unit spike patterns. After the tetrodes were adjacent to the cell layer, as indicated by the presence of multiunit activity, the tetrodes were settled into the cell layer for stable recordings.

Electrophysiological recording

All recordings were performed during a dark cycle (9:00 AM to 5:00 PM) on a day. Electrophysiological data were sampled at 2 kHz and low-pass filtered at 500 Hz. Unit activity was amplified and bandpass filtered at 500 Hz to 6 kHz. Spike waveforms above a trigger threshold (–60 μV) were timestamped and recorded at 30 kHz for 1.6 ms. To monitor the rat's moment-to-moment position, three red LEDs with a diameter of 5 mm were attached to the rat's back with a harness, and the positions of the LED signal were automatically tracked in real time at 25 Hz using a video camera attached to the ceiling.

Recordings from a novel run

In a recording day, the rat first rested in the rest box for 20 min, performed the same U track run (termed a familiar run) for 20 min as in the behavioral training, rested in the same box (termed a pre-rest period) for 60 min, and performed a novel U track run in a different room (termed a novel run) for 20 min. In this phase, the track was moved to a different room surrounded by curtains, which was 1 m apart from the familiar room. The rat was placed on the track so that the rat first experienced the different room with the same shape of

the track and rules as in the familiar run. Then, the rat was again rested in the same box (termed a post-rest period) for 60 min (Figure 1A). In the novel run, some rats were subjected to SWR disruption, as described below.

SWR disruption by closed-loop electrical stimulation

Upon the online detection of SWRs, closed-loop electrical stimulation was performed using extension code implemented on the Cerebus recording system (Blackrock) and custom-created C code[15]. A tetrode implanted into the hippocampus was chosen, and the envelope of its bandpass (100–400 Hz)-filtered LFP signals at 30 kHz was estimated in real time. The smoothed estimate of the envelope (env_{est}) of filtered LFP signals was computed as follows:

$$env_{est}(t) = env_{est}(t-1) + gain(t-1) * (|v_{bp}| - env_{est}(t-1)),$$

where

$$gain(t) = \begin{cases} 0.013, \text{if } |v_{bp}| \le env_{est}(t-1) \\ mean(gain(t-600), gain(t-599), \ldots, gain(t-1), 0.08), \text{if } |v_{bp}| > env_{est}(t-1) \end{cases},$$

and $|v_{bp}|$ denotes the absolute values of the filtered LFP signals. The length of the gain buffer was set to 600 (20 ms). Estimated values of smoothed mean ($mean_{est}$) and standard deviation (std_{est}) were then computed as follows:

$$mean_{est}(t) = mean_{est}(t-1) \times (N_{smooth} - 1) / N_{smooth} + |v_{bp}| / N_{smooth}$$

$$std_{est}(t) = \frac{(|v_{bp}| - mean_{est}(t-1))}{N_{smooth}} + std_{est}(t-1),$$

where N_{smooth} was the number of samples for smoothing (typically, set to be 150,000 in 500 ms). SWRs were detected online when the animals stayed in areas 15 cm from both ends of the track and when the envelope exceeded the detection threshold of 3 standard deviations above the estimated mean computed from LFP signals during periods in the rest box. At the time of SWR detection, an electrical pulse with a duration of 100 μs and an amplitude of 140–180 μA was applied to the vHC; the stimulation rate was limited to a maximum of 4 Hz. For delayed control stimulation, stimulation was applied with a latency of 250 ms after the onset of ripple detection so that the stimulation occurred outside the detected SWRs.

Histological analysis to confirm tetrode locations

After the experiments, the rats received an overdose of urethane and were intracardially perfused with 4% paraformaldehyde in PBS and decapitated. To aid in the reconstruction of the electrode tracks, the electrodes were not withdrawn from the brains until more than 3–4 hours after perfusion. After dissection, the brains were fixed overnight in 4% paraformaldehyde (PFA) and then equilibrated with a sequence of 20% sucrose and 30% sucrose in PBS. Frozen coronal slices (50 μm) were cut using a microtome, and serial sections were mounted and processed for cresyl violet staining. To perform cresyl violet staining, the slices were rinsed in water, counterstained with cresyl violet, and coverslipped with hydrophobic mounting medium. The positions of all the tetrodes were confirmed by identifying the corresponding electrode tracks in histological tissue with an optical microscope.

A spatial learning task

To reduce the number of animals, confirm the reproducibility of our study, and obtain further insights, we analyzed additional datasets from Igata et al. (2021). The data comprised spike trains of hippocampal pyramidal neurons recorded with tetrodes from 5 rats performing a spatial learning task. Briefly, a rat initiated a trial by nose poking in the start area (S) and obtained sucrose water during cue-sound presentation. Ten seconds after the onset of the sound presentation, the door after S was automatically opened, allowing the rat to enter the field. At the same time, 20 ml of chocolate milk reward was placed at a check point 1 (C_1). The rat ran from S to C_1, obtain the reward at C_1, and then ran from C_1 to the goal area (G) (path C_1-G). When the rat entered C_1, 5-kHz cue sounds were presented at 10 Hz for 0.3 s followed by continuous 10-kHz cue sounds until the rat reached G, helping a rat recognize that its current state was correct. When the rat took a correct path through C_1, the door before G (door 2) was opened so that the rat could enter G. In the goal area and the rat obtained 200 ml of chocolate milk reward. Twenty seconds after the onset of reward dispensation, the doors between G and peripheral alleyway (door 3) and the between the peripheral alleyway and S (door 4) were opened, allowing the rat to return to S to complete the trial. The next trial started when the rat again poked the reward port in the start area. On a recording day, the rats first performed the same task with a reward placed on C_1, termed the pre-learning phase. After several trials, the rewarded check point was moved from C_1 to a new check point 2 (C_2). In this phase, when the rat visited C_2, 5-kHz cue were played at 10 Hz for 0.3 s followed by continuous 10-kHz cue sounds were presented until the rat reached the goal area. After the reward replacement, the rats first exhibited trial-and-error behavior for several attempts to find an efficient trajectory, but they gradually learned to take the most efficient trajectory: path S-C_2-G. For more details, refer to Igata et al., 2021.

QUANTIFICATION AND STATISTICAL ANALYSIS

Definition of behavioral periods in the U track run

In the novel U track run, the run period was divided into two periods. Reward periods were defined when the rats stayed within areas less than 15 cm from both ends of the track for more than 2 s. Running periods were defined when the rats ran through the track area for more than 25 cm from both track ends. All laps including decelerating, stopping, or returning behavior were included for spike analyses.

Definition of behavioral periods in the spatial learning task

To analyze animal trajectory patterns, the open field was evenly divided into a 5 × 5 lattice and when animals were located onto five paths connecting specific areas (S, G, C_1, and C_2), paths S-C_1, C_1-G, C_2-G, S-C_2, and G-S were analyzed. Detailed results of behavioral patterns have been reported by Igata et al. (2021).

Spike sorting of hippocampal neurons

Spike sorting was performed offline using the graphical cluster-cutting software MClust. Rest recordings before and after the behavioral paradigms were included in the analysis to assure recording stability throughout the experiment and to identify hippocampal cells that were silent during the running behavior. Clustering was performed manually in two-dimensional projections of the multidimensional parameter space (i.e., comparisons between waveform amplitudes, waveform energies, and the principal components of waveforms, each measured on the four channels of each tetrode). Cluster quality was measured by computing the L_{ratio} and the isolation distance[34]. The L_{ratio} was computed by the original equation, proposed by Schmitzer-Torbert et al. (2005), not normalized by the total number of spikes recorded on the tetrode. A cluster was considered as a cell when the L_{ratio} was less than 0.20. In the autocorrelation histograms, cells with no clear refractory period (<3 ms) were excluded from analyses. Cells with spike waveforms longer than 300 μs and an average firing rate of less than 3 Hz throughout an entire recording period were considered putative excitatory cells and included in the analysis.

Between place cells and non-place cells, no significant differences were found in maximum waveform amplitudes in a channel with the largest amplitude (place cells: n = 279 cells, 130.5 ± 2.0 μV; non-place cells: n = 109 cells, 126.5 ± 3.1 μV; Z = 0.93, P = 0.35, Mann–Whitney U test) and in L_{ratio} (place cells: n = 279 cells, 0.11 ± 0.0039; non-place cells: n = 109 cells, 0.099 ± 0.0061; Z =1.61, P = 0.11, Mann–Whitney U test). Overall, place cells had significantly higher mean firing rates than non-place cells (place cells: n = 279 cells, 0.62 ± 0.05 Hz; non-place cells: n = 109 cells, 0.36 ± 0.06 Hz; Z = 5.38, P = 7.3 × 10^{-8}, Mann–Whitney U test).

Spatial firing patterns

For analyzing spike patterns in the U track run, the animal's coordinates and the positions of spikes of individual cells were projected onto a centerline of alleyways corresponding to each trajectory. In each run, the average firing-rate distribution on each trajectory ("R1 to R2" or "R2 to R1") was separately computed along the projected line by dividing the total number of spikes in each location bin (10 cm) by the total time that the rat spent in that bin. Reward periods were excluded from this calculation. All firing-rate distributions were smoothed by a one-dimensional convolution with a Gaussian kernel with a standard deviation of one pixel (10 cm). A cell was defined as a place cell in a direction based on the two following criteria: (1) the average firing-rate distribution on a trajectory in a session had a maximum firing rate of more than 0.5 Hz (i.e., the absolute maximum firing rate), and (2) the maximum firing rate exceeded 2 standard deviations (SDs) above the mean, where the SD and the mean were computed from the series of firing rates except the maximum firing rate in that distribution. The other cells that did not meet the criteria were classified as non-place cells. For each place cell, a place field center in a direction was defined as the position giving the maximum firing rate in the distribution. Under this criterion, some place cells had one place field in either one of two trajectories, whereas the others had two place fields, one in each trajectory. For a given place cell pair, the distance between the two place field centers in a direction was computed, termed the place field distance. If a place cell pair had bidirectional place fields in both directions, a smaller place field distance in a direction was considered as a place field distance for the pair. Place cell pairs with place field distances less than 30 cm and more than 60 cm were classified as close and distant place cell pairs, respectively.

For analyzing spike patterns in the spatial learning task, the average firing rate on each path was separately computed by dividing the total number of spikes in each path by the total time that the rat spent in that path. Reward periods were excluded from this calculation. A cell was defined to encode a path if an average firing rate on the path was 0.5 Hz. Neurons that specifically encoded pre-existing information (path S-C_1-G-S) in the pre-learning phase and novel information (path S-C_2-G) in the learning phase were classified into new and old cells, respectively. Neurons that encoded both information were classified into both cells, and the other neurons that did not encode any information were classified into none cells.

Detection of synchronous events and SWRs

During rest and reward periods in the linear track run and stop periods in the spatial learning task, synchronous events were detected at least three cells were simultaneously activated in a time window of 100 ms that was preceded by >200-ms of silence. To compute

sequence scores for replay analysis, this time window was set to be 200 ms. The electrode including the largest number of putative pyramidal cells identified in the spike sorting process was used for SWR detection. LFP signals were bandpass filtered at 150–250 Hz, and the root mean-square was calculated with a bin size of 10 ms. SWR events were detected if the power exceeded a threshold for at least 15 ms. The threshold for SWR detection was set to 3 standard deviations (SDs) above the mean of all envelopes computed from the run or rest periods. The onset of SWRs was marked at the point when the root mean-square first exceeded 3 SDs above the mean.

Definition of replay events

Uniform prior Bayesian decoding was applied to estimate the animals' positions from the spike trains[15]. The spatial firing-rate distributions of individual place cells were used as position-tuning curves. Assuming Poisson firing statistics and a uniform prior over position, the posterior probability of the animal's location (*loc*) in a time window (τ) including neuronal spike patterns (*s*) was computed as follows:

$$Pr(loc|s) = U \Big/ \sum_{j=1}^{L} U$$

where

$$U = \left(\prod_{i=1}^{N} f_i(loc)^{n_i} \right) \exp\left(-\tau \sum_{i=1}^{N} f_i(loc) \right),$$

$f_i(loc)$ is the position tuning curve of the i-th neuron, and N and L are the total numbers of neurons and total location bins, respectively. The time window τ was set to 20 ms to estimate the animal's positions.

Sequence scores were defined for individual synchronous events as described previously[29]. The data from rats with at least 27 cells were analyzed. For the represented path segments, $Pr(loc|s)$ constructed from a synchronous event was smoothed over time bins with a Gaussian filter (σ = 10 ms). In the filtered $Pr(loc|s)$, a maximum a posteriori probability (MAP) was computed as the largest posterior probability across all positions per time bin[35], and the time bins with MAPs greater than ($2 \times 1/n_{loc\ bin}$) were included for the analysis, where $n_{time\ bin}$ and $n_{loc\ bin}$ were the numbers of time and location bins in the synchronous event, respectively. If the number of time bins in which MAP exceeded the threshold was less than 3, all the time bins were analyzed. $Pr(loc|s)$ was normalized within the synchronous event as follows:

$$normPr(loc|s) = \frac{Pr(loc|s)}{\sum_{i=1}^{n_{loc\ bin}} Pr\ (loc_i|s)}.$$

A sequence score *r(loc, time; normPr)* representing the weighted correlation between time and location was computed as follows:

$$r(loc, time, normPr) = \frac{cov(loc, time; normPr)}{\sqrt{cov(loc, loc; normPr)cov(time, time; normPr)}},$$

where

$$m(loc; normPr) = \frac{\sum_{i=1}^{n_{time\ bin}} \sum_{j=1}^{n_{loc\ bin}} normPr_{ij} loc_j}{\sum_{i=1}^{n_{time\ bin}} \sum_{j=1}^{n_{loc\ bin}} normPr_{ij}}$$

$$cov(loc; time; normPr) = \frac{\sum_{i=1}^{n_{time\ bin}} \sum_{j=1}^{n_{loc\ bin}} normPr_{ij}(loc_j - m(locj; normPr))(time_i - m(time; normPr)}{\sum_{i=1}^{n_{time\ bin}} \sum_{j=1}^{n_{loc\ bin}} normPr_{ij}}.$$

Synchronous events with an $|r| \geq 0.5$ were considered replay events, and the replay directions were determined by the signs of the correlations *r*, where positive and negative correlations of *r* represent forward and backward replay directions, respectively.

Similarity of synchronous events

To quantify the similarity of synchronous events, each synchronous event in the reward and rest periods was converted to an *N*-dimensional vector containing 1 or 0 depending on whether each neuron showed spikes or not during the event, where *N* denotes the total number of neurons. Pearson correlation coefficients or Jaccard similarity coefficients between all possible vector pairs were calculated to construct a sync-to-sync correlation matrix. To evaluate whether Jaccard similarity coefficients in individual rats were

significant, neuronal spike patterns within each synchronous event were shuffled across neurons. For quantification, 100 shuffled datasets were created to obtain the distribution of coefficients and their averaged values.

Uniform manifold approximation and projection (UMAP)

Supervised UMAP was performed using a Matlab function "run_umap" (available at https://umap-learn.readthedocs.io/en/latest/basic_usage.html). With UMAP, *N*-dimensional vectors from individual synchronous events were reduced to two dimensions with the following hyperparameters: *n_neighbors* = 4, *min_dist* = 0.2, *n_components* = 2, and *metric* = 'distance'. A cluster was classified into a reward (familiar) or a reward (novel) cluster if the cluster included a higher proportion of reward-associated synchronous events in the familiar or novel run, respectively.

Per-cell contribution to synchronous events (CC)

To statistically determine whether each neuron significantly changed its contribution to synchronous events from the pre-rest to the post-rest periods, we computed CCs in reference to a previous study[29]. For each neuron, 100 surrogate datasets were created by randomly shuffling its inter-spike intervals (ISIs) in each rest period. This shuffling procedure randomized the temporal correlation of spikes across neurons without altering the total spike count within each neuron. The CC of cell *i* to event *e* was computed as follows:

$$CC_{e,i} = Nsync_e - Nsync_{e,i}(shuffle)$$

where $Nsync_e$ is the number of activated cells in event *e* and $Nsync_{e,i}(shuffle)$ is the averaged $Nsync_e$ obtained from the 100 shuffled spike patterns of cell *i*.

To assess whether a cell showed a significant increase/decrease in CCs in the post-rest period, compared with those in the pre-rest period, a paired t test was applied to CCs computed from all synchronous events between the pre- and post-rest periods ($P < 0.05$). For each cell, the CCs were averaged over all events and presented as a single value (e.g. Figures 1E–1G).

Definition of more/less-participating neurons

To assess whether a cell showed a significant increase/decrease in a participation rate in reward-associated synchronous events in the novel run, compared with that in the familiar run, a chi-square test was applied to its participation rates between the familiar and novel runs ($P < 0.05$). More- and less-participating neurons were defined as neurons showing significantly higher and lower participation rates in the novel run, respectively.

Spike correlations in a cell pair

To measure the degree to which a given cell pair exhibited synchronous firing, the numbers of spikes were counted in consecutive 50-ms windows in each of the two cells, creating N-dimensional vectors x and y, where N is the total number of windows. Pearson correlation coefficients were computed between the two vectors as follows:

$$Correlation = \frac{\sum_{i=1}^{N}(x_i - \bar{x})(y_i - \bar{y})}{\sqrt{\sum_{i=1}^{N}(x_i - \bar{x})^2}\sqrt{\sum_{i=1}^{N}(y_i - \bar{y})^2}}$$

Silent cells were defined as cells with a firing rate of less than 0.02 Hz and correlations of cell pairs including at least one silent cell were computed as 0.

To compute correlations during synchronous events in the rest periods and reward periods, a N-dimensional vector was computed for each cell with entries of +1 or 0 depending on whether or not the cell emitted spikes in the event, respectively, where N is the total reward-associated synchronous events. Pearson correlation coefficients were computed between the two vectors.

To evaluate whether a neuronal pair showed a significant difference in correlations from the pre-rest period to the post-rest period ($correlation_{pre}$ to $correlation_{post}$), a difference in Fisher's z-transformed value was computed as follows:

$$Z = \frac{\frac{1}{2}\log\frac{1+\text{correlation}_{post}}{1-\text{correlation}_{post}} - \frac{1}{2}\log\frac{1+\text{correlation}_{pre}}{1-\text{correlation}_{pre}}}{\sqrt{\frac{1}{n_{post}-3}+\frac{1}{n_{pre}-3}}}$$

where n_{pre} and n_{post} were the numbers of bins computed for $correlation_{pre}$ and $correlation_{post}$, respectively. Cell pairs with ΔFisher's *Z* that gave a significance level below a certain *P* value ($P = 0.05./(N_{pair} \times N_{pair})$), where N_{pair} was the total number of cell pairs, were defined to exhibit increased or decreased correlations from the pre-rest period to the post-rest period.

Statistical analysis

For all statistical tests, no exclusions of rats were performed. As all the data and influences in this study were analyzed and generated completely independently, blinding was not applicable as there was no bias present.

All the data were analyzed using MATLAB. The data are presented as dot plots, distributions, or box plots. Comparisons of two-sample data were analyzed using *t* test or Mann–Whitney U tests. Comparisons of two proportions were analyzed using chi-square test. Multiple group comparisons were performed by post hoc Bonferroni corrections. For within-group comparisons, the same statistical tests were confirmed from the datasets in Figures 1E–1G, 2D, 3J, 4E, 4H, 6G, and 6I, after excluding a rat in each group (Table S2). For across-group comparisons, the same statistical tests were applied to datasets in Figures 1H, 3F, and 4F, after excluding a rat in each group (Figure S6). In these figures, statistical significance was reported only when the datasets withstood this leave-one-out procedure. The null hypothesis was rejected at the $p < 0.05$ level, unless otherwise specified.